This document is written by Dr. Tong Huang, and it serves as supplementing materials of the manuscript titled "A Non-intrusive Decentralized Approach to Stabilizing IBR-dominated AC Microgrids" submitted to IEEE Transactions on Power Systems, in order to meet the page limit requirement of the journal. The index system of sections, equations, and figures in this document is consistent with the one used in the manuscript. For example, "Figure 1" in this document refers to "Figure 1" of the submitted manuscript.

APPENDIX A
DYNAMICS OF GRID-FORMING IBRS

Suppose that the n-th IBR is grid-forming. As shown in Figure 1, the GFM IBR includes a DC voltage source, an inverter, a resistor-inductor-capacitor (RLC) low-pass filter, a power controller, a voltage controller, and a current controller. The dynamics of each block in Figure 1 is introduced as follows.

1) RLC filter: The inverter connects to the rest of the microgrid via an RLC filter whose dynamics are [29]

$$L_{\mathrm{f}n}\dot{i}_{\mathrm{ld}n} = -r_{\mathrm{f}n}i_{\mathrm{ld}n} + L_{\mathrm{f}n}\omega_0 i_{\mathrm{lq}n} + v_{\mathrm{id}n} - v_{\mathrm{od}n} \tag{26a}$$
$$L_{\mathrm{f}n}\dot{i}_{\mathrm{lq}n} = -r_{\mathrm{f}n}i_{\mathrm{lq}n} - L_{\mathrm{f}n}\omega_0 i_{\mathrm{ld}n} + v_{\mathrm{iq}n} - v_{\mathrm{oq}n} \tag{26b}$$
$$C_{\mathrm{f}n}\dot{v}_{\mathrm{od}n} = C_{\mathrm{f}n}\omega_0 v_{\mathrm{oq}n} + i_{\mathrm{ld}n} + i_{\mathrm{od}n} \tag{26c}$$
$$C_{\mathrm{f}n}\dot{v}_{\mathrm{oq}n} = -C_{\mathrm{f}n}\omega_0 v_{\mathrm{od}n} + i_{\mathrm{lq}n} + i_{\mathrm{oq}n} \tag{26d}$$

where $i_{\mathrm{ld}n}$ and $i_{\mathrm{od}n}$ ($i_{\mathrm{lq}n}$ and $i_{\mathrm{oq}n}$) are the direct (quadrature) component of the current $\mathbf{i}_{\mathrm{l}n}$ and $\mathbf{i}_{on}$ annotated in Figure 1; $v_{\mathrm{id}n}$ and $v_{\mathrm{od}n}$ ($v_{\mathrm{iq}n}$ and $v_{\mathrm{oq}n}$) are the direct (quadrature) components of the voltage $\mathbf{v}_{\mathrm{i}n}$ and $\mathbf{v}_{on}$; resistance $r_{\mathrm{f}n}$, inductance $L_{\mathrm{f}n}$, and capacitance $C_{\mathrm{f}n}$ of the RLC circuit are labeled in Figure 1; and ω_0 is the nominal frequency (i.e., 377 or 314 rad/s). Note that the reference positive direction of $\mathbf{i}_{on}$ is *pointing into* the IBR.

2) Power controller: A power controller contains a power calculator, a power filter, and a droop controller. The power calculator computes the instantaneous real power $\tilde{p}_n$ and reactive power $\tilde{q}_n$ *injecting into* the rest of the microgrid, based on IBR n's terminal voltages ($v_{\mathrm{od}n}$ and $v_{\mathrm{oq}n}$) and current ($i_{\mathrm{od}n}$ and $i_{\mathrm{oq}n}$) in the direct-quadrature (d-q) reference frame of IBR n. With the positive reference directions assigned to $\mathbf{v}_{on}$ and $\mathbf{i}_{on}$ in Figure 1, $\tilde{p}_n$ and $\tilde{q}_n$ are computed by

$$\tilde{p}_n = -\frac{3}{2}(v_{\mathrm{od}n}i_{\mathrm{od}n} + v_{\mathrm{oq}n}i_{\mathrm{oq}n}) \tag{27a}$$
$$\tilde{q}_n = -\frac{3}{2}(v_{\mathrm{oq}n}i_{\mathrm{od}n} - v_{\mathrm{od}n}i_{\mathrm{oq}n}). \tag{27b}$$

The instantaneous real and reactive power feed the power filter, i.e., a digital low-pass filter, whose dynamics is described by

$$\dot{P}_n = -\omega_{\mathrm{c}n}P_n + \omega_{\mathrm{c}n}\tilde{p}_n \tag{28a}$$
$$\dot{Q}_n = -\omega_{\mathrm{c}n}Q_n + \omega_{\mathrm{c}n}\tilde{q}_n \tag{28b}$$

where $\omega_{\mathrm{c}n}$ is the cut-off frequency; and P_n and Q_n are the real and reactive power filtered by the power filter. The droop controller takes P_n and Q_n as inputs and it specifies frequency ω_n, phase angle δ_n and voltage setpoints $v^*_{\mathrm{od}n}$ and $v^*_{\mathrm{oq}n}$ via

$$\dot{\delta}_n = \omega_n - \omega_0, \quad \omega_n = \omega_{\mathrm{s}n} - \alpha_n P_n \tag{29a}$$
$$v^*_{\mathrm{od}n} = V_{0n} - \beta_n Q_n, \quad v^*_{\mathrm{oq}n} = 0 \tag{29b}$$

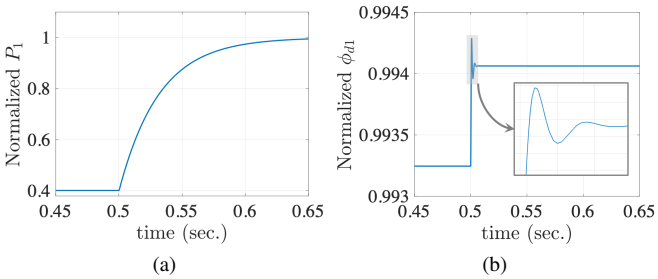

Fig. 20. Time-domain evolution of normalized P_1 and $\phi_{\mathrm{d}1}$.

where $\omega_{\mathrm{s}n}$ is set by a secondary controller; V_{0n} is a voltage setpoint; and α_n and β_n are droop control parameters. The angle δ_n is used in the Park and the inverse Park transformations that bridge three-phase variables with variables in the d-q-0 frame.

3) Voltage controller: The dynamics of the voltage controller is governed by

$$\dot{\phi}_{\mathrm{d}n} = -v_{\mathrm{od}n} + v^*_{\mathrm{od}n}, \quad \dot{\phi}_{\mathrm{q}n} = -v_{\mathrm{oq}n} + v^*_{\mathrm{oq}n}, \tag{30a}$$
$$i^*_{\mathrm{ld}n} = K_{\mathrm{pv}n}(v^*_{\mathrm{od}n} - v_{\mathrm{od}n}) - F_n i_{\mathrm{od}n} - \omega_0 C_{\mathrm{f}n} v_{\mathrm{oq}n} + K_{\mathrm{iv}n}\phi_{\mathrm{d}n} \tag{30b}$$
$$i^*_{\mathrm{lq}n} = K_{\mathrm{pv}n}(v^*_{\mathrm{oq}n} - v_{\mathrm{oq}n}) - F_n i_{\mathrm{oq}n} + \omega_0 C_{\mathrm{f}n} v_{\mathrm{od}n} + K_{\mathrm{iv}n}\phi_{\mathrm{q}n} \tag{30c}$$

where $\phi_{\mathrm{d}n}$ and $\phi_{\mathrm{q}n}$ are state variables for the voltage controller; $i^*_{\mathrm{ld}n}$ and $i^*_{\mathrm{lq}n}$ are setpoints of the current controller provided by the voltage controller; and $K_{\mathrm{pv}n}$, F_n, and $K_{\mathrm{iv}n}$ are control parameters.

4) Current controller: The dynamics of the current controller is described by

$$\dot{\gamma}_{\mathrm{d}n} = -i_{\mathrm{ld}n} + i^*_{\mathrm{ld}n}, \quad \dot{\gamma}_{\mathrm{q}n} = -i_{\mathrm{lq}n} + i^*_{\mathrm{lq}n}, \tag{31a}$$
$$v^*_{\mathrm{id}n} = K_{\mathrm{pc}n}(i^*_{\mathrm{ld}n} - i_{\mathrm{ld}n}) - \omega_0 L_{\mathrm{f}n} i_{\mathrm{lq}n} + K_{\mathrm{ic}n}\gamma_{\mathrm{d}n} \tag{31b}$$
$$v^*_{\mathrm{iq}n} = K_{\mathrm{pc}n}(i^*_{\mathrm{lq}n} - i_{\mathrm{lq}n}) + \omega_0 L_{\mathrm{f}n} i_{\mathrm{ld}n} + K_{\mathrm{ic}n}\gamma_{\mathrm{q}n} \tag{31c}$$

where $\gamma_{\mathrm{d}n}$ and $\gamma_{\mathrm{q}n}$ are state variables for the current controller; and $K_{\mathrm{pc}n}$, and $K_{\mathrm{ic}n}$ are control parameters.

5) Time scale separation: The state variables of dynamics (26), (28), (29), (30), and (31) include δ_n, P_n, Q_n, $\phi_{\mathrm{d}n}$, $\phi_{\mathrm{q}n}$, $\gamma_{\mathrm{d}n}$, $\gamma_{\mathrm{q}n}$, $i_{\mathrm{ld}n}$, $i_{\mathrm{lq}n}$, $v_{\mathrm{od}n}$, and $v_{\mathrm{oq}n}$. Define $\mathcal{S}^{\mathrm{s}}_n = \{\delta_n, P_n, Q_n\}$ and $\mathcal{S}^{\mathrm{f}}_n = \{\phi_{\mathrm{d}n}, \phi_{\mathrm{q}n}, \gamma_{\mathrm{d}n}, \gamma_{\mathrm{q}n}, i_{\mathrm{ld}n}, i_{\mathrm{lq}n}, v_{\mathrm{od}n}, v_{\mathrm{oq}n}\}$. Next we show that the states in $\mathcal{S}^{\mathrm{f}}_n$ can be stabilized much faster than those in $\mathcal{S}^{\mathrm{s}}_n$ via simulating a grid-connected IBR with a representative parameter setting [29]. In the simulation[2], the load changes at time $t = 0.5$s, Figure 20 visualizes state variables P_1 and $\phi_{\mathrm{d}1}$. It can be observed that it takes more than 0.15s to stabilize P_1, while $\phi_{\mathrm{d}1}$ is stabilized around 0.006s after the disturbance occurs. Figure 21 presents the stabilization time of key variables of the IBR. Figure 21 suggests that ω_1, P_1, and Q_1 are stabilized much slower than the states in $\mathcal{S}^{\mathrm{f}}_n$. A similar observation is also reported in [38].

A very large body of literature (see [4] and the references therein) studies the slow dynamics defined by the states in $\mathcal{S}^{\mathrm{s}}_n$ by assuming that the fast states in $\mathcal{S}^{\mathrm{f}}_n$ are stabilized fast.

[2]Figures 20 and 21 are obtained by simulating Microgrid 1 in Figure 12. The per-phase impedance at Load 1 changes from 25Ω to 10Ω at $t = 0.5$s.

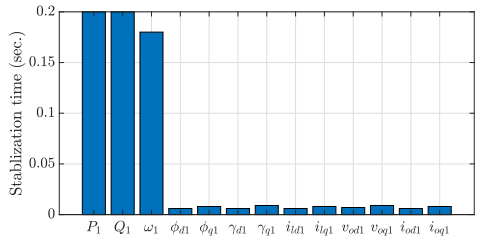

Fig. 21. Stabilization time of key variables

This paper examines the interaction among the fast states in $\mathcal{S}_n^{\text{f}}$ by assuming the states in $\mathcal{S}_n^{\text{s}}$ as constants. With such an assumption, we exclude the dynamics of the slow states in $\mathcal{S}_n^{\text{s}}$ to derive (1).

APPENDIX B
DYNAMICS OF GRID-FOLLOWING IBRS

Suppose that the $n-$th IBR is grid-following (GFL). The cyber-physical architecture of the GFL IBR is summarized in Figure 2. The dynamics of the RLC output filter and the current controller in Figure 2 can be characterized by (26) and (31). Next, we elaborate the phase locked loop (PLL) and the block that generates the current set points for the current controller.

1) Phase locked loop: The PLL aims to track the frequency of the grid that hosts the GFL IBR. This is done by a proportional-integral (PI) controller described by

$$\dot{\eta}_n = K_{\text{ip}n} v_{\text{oq}n} \tag{32a}$$

$$\omega_n = \eta_n + K_{\text{pp}n} v_{\text{oq}n} + \omega_0 \tag{32b}$$

where η_n is the state variable of the PLL; and $K_{\text{ip}n}$ and $K_{\text{pp}n}$ are control parameters. The integral of ω_n is used in the Park and inverse Park transformation.

2) The block generating current set points: Given the real and reactive power set points (P_{n}^* and Q_{n}^*), the current set points ($i_{\text{ld}n}^*$ and $i_{\text{lq}n}^*$) are produced by the following algebraic equations:

$$i_{\text{ld}n}^* = -\frac{2}{3}\frac{P_n^*}{v_{\text{od}n}}, \quad i_{\text{lq}n}^* = \frac{2}{3}\frac{Q_n^*}{v_{\text{od}n}}. \tag{33}$$

Equation (33) is linearized to derive (1) for the GFL IBRs.

The simulation parameters in Section V-A1 for the GFL IBR are as follows: $L_{\text{f1}} = 1.35$mH, $C_{\text{f1}} = 50\mu$F, $r_f = 0.1\Omega$, $K_{\text{ip1}} = 2.14$, $K_{\text{pp1}} = 0.37$, $P_1^* = 2500$W, and $Q_1^* = 0$.